ELSEVIER

Contents lists available at ScienceDirect

International Journal of Non-Linear Mechanics

journal homepage: www.elsevier.com/locate/nlm



Analytical solutions for a conical elastic sheet under a live normal load

Jaspreet Singh, Prashant K. Purohit *

Department of Mechanical Engineering and Applied Mechanics, University of Pennsylvania, Philadelphia, PA 19104, USA



ARTICLE INFO

Keywords: Cone Isometric deformations Elliptic functions

ABSTRACT

We study the isometric conical deformation of an inextensible elastic sheet in response to a distributed external loading that is normal to the deformed sheet. The sheet is planar in the reference configuration and it deforms into a cone with a flower-shaped cross-section under load. These deformed configurations are distinguished by the number of lobes. We focus on the geometry and energetics of various lobed-cones in the deformed configuration and discuss their relative stability. First, we assume that the displacements are small which leads to linear governing equations for the curvature that we solve analytically to yield sinusoidal solutions. Then, we relax this restriction on the magnitude of the displacement which leads to nonlinear governing equations, which we again solve analytically using Jacobi elliptic functions which are periodic but not sinusoidal. We show that the sinusoidal solution can be recovered in the limit that the external loads are small.

1. Introduction

Interest in the mechanics of elastic sheets stems partly from their diverse engineering applications in structural design [1,2], and partly from the observation that the analysis of relatively unremarkable physical phenomena, such as crumpling of paper and draping of textiles, is rooted in ideas from differential geometry and elasticity [3,4]. A common theme that spans the study of elastic sheets and their applications is that small strains can cause relatively large deformations, resulting in nonlinear governing equations. These can be linearized, provided certain restrictions on strains, displacements, and curvatures are satisfied [1,2].

The kinematics of elastic sheets is conventionally described in terms of the deformation of a midplane. For a sheet described by convected coordinates (ξ_1,ξ_2,z) , where z is along the thickness, Kirchhoff's hypothesis [1,2] relates the linearized strains $E_{\alpha\beta}$ at any point (ξ_1,ξ_2,z) in the sheet to the strains $\bar{E}_{\alpha\beta}$ of the corresponding point $(\xi_1,\xi_2,0)$ on the midplane such that,

$$E_{\alpha\beta}(\xi_1,\xi_2,z) = \bar{E}_{\alpha\beta}(\xi_1,\xi_2) \ + \ z \ \kappa_{\alpha\beta}(\xi_1,\xi_2) \ + O(z^2),$$

where $\alpha, \beta = 1, 2$, and $\kappa_{\alpha\beta}$ are the curvatures. This decomposition is fundamental to the study of the mechanics of elastic plates [5].

For thin sheets subjected to *amenable* boundary conditions, the in-plane strains $\bar{E}_{\alpha\beta}$ are negligible, and the sheet deforms by out-of-plane bending, quantified by the curvatures $\kappa_{\alpha\beta}$. Amenable boundary conditions are important because for certain boundary conditions that involve pure stretching the in-plane strains are not negligible. Nevertheless, the scope of the description is enormous and includes various interesting phenomena such as the buckling of a plane sheet in response

Although a bulk of scholarship has been devoted to studying isometric deformations, we mention only a few recent studies here and refer the reader to [5,8] for an exhaustive review. Cerda and Mahadevan [9] have successfully used an idealized inextensible elastic sheet model to study the wrinkling patterns in the human skin. King et al. [10] studied the wrinkling patterns in an elastic sheet from a similar perspective and concluded that beyond a certain confinement symmetric wrinkling is susceptible to a localized crumpling. At the micrometer scale, the mechanics of lipid bilayer membranes [11-13] is governed by the principle that the observed morphology minimizes the elastic bending energy. Rim et al. [14] exploited this idea to compute equilibrium configurations for a vesicle in cylindrical confinement to highlight how the interplay between adhesion and confinement can result in highly curved organelle shapes in various cells. Apart from this, differential growth of thin shells can result in many intricate morphologies [15–17], which has extensive applications in understanding biological shape evolution such as blooming flowers and curling leaves. Efficient packing of flat sheets also has applications in origami inspired structural design [18–20].

E-mail address: purohit@seas.upenn.edu (P.K. Purohit).

to a compressive load, snap-through of a thin shell [1], packing of flat sheets in a cylindrical confinement [3], crumpling of a paper [6], and draping of a tablecloth [7]. When the in-plane strains are zero, the deformed configuration of the sheet is isometric to the reference configuration which implies that both the metric and the Gauss curvature remain unchanged. We refer to such deformations as *isometric* deformations. In these cases, since the in-plane strains are zero, the corresponding stress conjugates are Lagrange multipliers and the elastic energy consists of only the bending energy.

^{*} Corresponding author.

Folding of a flat elastic sheet into a conical configuration is well studied in the literature [3,5]. The deformed conical configuration is isometric to the original flat sheet and has zero Gauss curvature everywhere except at the apex. This concept has been used to study gravity induced draping [7] and crumpling of paper [21]. A salient aspect of conical deformations is the study of stress concentrations around the apex of the cone. Near the apex, also referred to as a singularity, the assumption that the sheet is inextensible breaks down; the size and properties of this zone depend upon the packing fraction of the sheet [4,6,22]. A common example of the stress and curvature localization in an elastic sheet is in crumpling of a plane sheet of paper [6,23]. An in-depth study of the creases and ridges in crumpled paper is available in Blair and Kudrolli [23], but is beyond the scope of this paper. Here we are interested in investigating the response of a thin inextensible elastic sheet placed on a sharp end, subject to a distributed external load (see Fig. 1). The sheet is flat in the reference configuration. As the sheet deforms, it curls up on itself which results in a q-lobed flower-shaped configuration as shown in Fig. 1. This is an example of the well-studied isometric deformation [3.7] transforming a flat sheet into a conical configuration while conserving the metric and the Gauss curvature. Several ideas involving the general kinematics of the conical deformation [3,4,7] and the derivation of the governing equations using energy minimization principles [5,14] are based on previous works. However, the live loading normal to the deformed shape of the plate considered in this paper has not been described elsewhere. We show that under such specialized external loads it is possible to obtain analytical solutions for the shapes of conical plates which are similar to the lobed shapes of buckled cylindrical shells. We investigate the geometrical characteristics of various lobed configurations. We examine the dependence of stress distribution on the radial and angular coordinates. Finally, we compute the potential energy of the various shapes and comment on their relative stability.

2. Approach

Our objective is to study the deformation of a thin developable elastic sheet placed on a pointed end subjected to a distributed force $p(r, \theta)$, as shown in Fig. 1. The sheet, planar in the reference configuration, is described by a set of two convected coordinates, r and θ . In the deformed configuration, the sheet is conical where each cross-section is shaped like a *q*-lobed flower, as shown in Fig. 1. We investigate the geometrical characteristics of the cone such as curvature, transverse displacement $w(r, \theta)$, and shape of the cross-section, in the deformed configuration.

The paper is divided into two parts:

- · Part 1: Small deflections: In this part, we assume that the deflection angle (see Fig. 1) $\alpha \ll 1$, which leads to linear governing equations [3]. The loading $p(r, \theta) = p(r)$ is axisymmetric and independent of θ . To get the deformation profiles, we minimize the potential energy functional. Our key result here is that the curvature of the cone in the deformed configuration is sinusoidal.
- Part 2: Finite deflections: This part aims to extend the work in part 1 to finite deflections ($\alpha \sim O(1)$), resulting in nonlinear governing equations. Again, the loading $p(r,\theta) = p(r)$ is axisymmetric and independent of θ . Here, the curvature of the cone in the deformed configuration is described using Jacobi Elliptic functions [24], which are periodic but not sinusoidal.

We assume that the elastic sheet is inextensible, hence the cone in the deformed configuration is always isometric to a flat sheet. This assumption has three key consequences: (i) the Gauss curvature of the plate remains constant (= 0) during the deformation, (ii) no in-plane extension takes place, hence the in-plane strains $\varepsilon_{rr}, \varepsilon_{\theta\theta}$ and $\varepsilon_{\theta r}$ are zero, whereas the corresponding stress conjugates are indeterminate Lagrange multipliers, and (iii) the elastic energy of the plate solely consists of the bending energy. Where appropriate, we use geometrically nonlinear shell theory [1,3,25].

3. Part 1: Small deflections

In this section, we solve the problem posed above for small deflection ($\alpha \ll 1$) by minimizing the potential energy functional for the system. The first step is to compute the elastic energy of the sheet. We proceed by assuming that the transverse displacement w = $rg(\theta)$ — characteristic of a conical deformation [5]. We compute the curvatures, which are in turn used to compute the bending energy. Note that the sheet is inextensible, hence there is no energetic contribution from stretching. The second step is to account for the constraint of inextensibility using Lagrange multipliers. The third step is to compute the work done by external loading $p(r,\theta)$. These steps enable us to compute the functional to be minimized. We calculate the variation of the energy functional and set it to zero to get the governing equations describing the deformation.

3.1. Analysis

We use curvilinear coordinates, r, θ where 0 < r < R and $0 < \theta < 2\pi$ to parametrize the sheet in the undeformed configuration. We give the symbols used in this section in Table 1. The displacement of the sheet parallel to the fixed support is $w(r, \theta)$ and the profile is conical:

$$w(r,\theta) = rg(\theta). \tag{1}$$

The curvature components κ_r , κ_θ and $\kappa_{r\theta}$ comprising the second fundamental form (see Ref. [3]) are obtained as follows [25]:

$$\begin{split} \kappa_{\theta} &= -\frac{w_{\theta\theta}}{r^2} - \frac{w_r}{r} = -\frac{1}{r}(g'' + g), \quad \kappa_r = -w_{rr} = 0, \\ \kappa_{r\theta} &= -\frac{w_{r\theta}}{r} + \frac{w_{\theta}}{r^2} = 0. \end{split} \tag{2}$$

Note that $()'=\frac{\partial}{\partial\theta},\ ()''=\frac{\partial^2}{\partial\theta^2}$ and so on. The next step is to compute the bending energy in terms of the curvature κ_r, κ_θ and $\kappa_{r\theta}$ [3]. The elastic energy per unit reference area of the sheet is e_h .

$$e_b = \frac{1}{2} \left(m_r \kappa_r + m_\theta \kappa_\theta + m_{r\theta} \kappa_{r\theta} \right) = \frac{B}{2} (\kappa_r + \kappa_\theta)^2 + B(1 - \nu)(\kappa_{r\theta} - \kappa_r \kappa_\theta) = B \frac{(g'' + g)^2}{2r^2},$$
(3)

where h and v are the thickness and Poisson ratio of the sheet respectively, and, $B=\frac{Eh^3}{12(1-v^2)}$ where E is the Young's modulus. We have to integrate e_b over the area of the elastic sheet ($\varepsilon < r < R$, $0 < \theta < 2\pi$) in the reference configuration to compute the total elastic energy E_h . Here, ε is the size of the boundary layer for the singularity at the center [4]. In the region $0 < r < \varepsilon$, our assumptions that the sheet is elastic and inextensible break down [4,5]. The elastic energy is,

$$E_b = \int_{\varepsilon}^{R} \int_{0}^{2\pi} e_b \, r dr d\theta = \frac{1}{2} B \log \frac{R}{\varepsilon} \int_{0}^{2\pi} (g'' + g)^2 d\theta. \tag{4}$$

The work done by external loads W_{ext} is,

$$\begin{split} W_{ext} &= \int_{\varepsilon}^{R} r dr \int_{0}^{2\pi} d\theta \ p(r) w(r,\theta) = \int_{0}^{2\pi} g d\theta \int_{\varepsilon}^{R} p(r) r^{2} dr \\ &= P \int_{0}^{2\pi} g d\theta, \end{split} \tag{5}$$

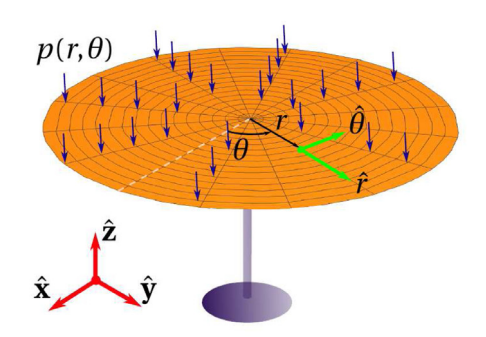
where $P = \int_{\varepsilon}^{R} p(r)r^2 dr$.

To account for the inextensibility, the following constraint equation involving $g(r, \theta)$ must be added to the potential energy functional (for detailed derivation see Ref. [4]).

$$I = \frac{1}{2} \int_{0}^{2\pi} d\theta \ (g'^2 - g^2) = 0. \tag{6}$$

The physical meaning of the above equation is that the perimeter of the locus of points at a fixed distance r from the tip in the reference configuration is $2\pi r$, which is invariant under isometric deformations.

Reference Configuration



Deformed Configuration

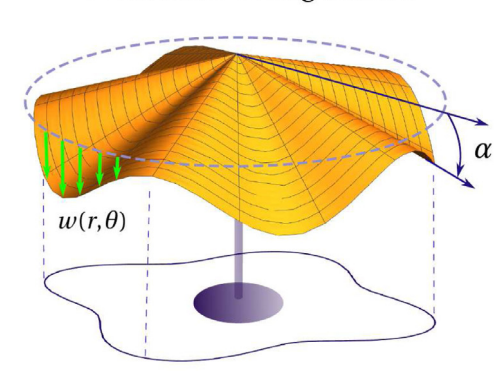


Fig. 1. We consider an elastic sheet, flat in the reference configuration parametrized by convected coordinates r and θ , subjected to a loading $p(r,\theta)$. We assume that the sheet is inextensible and is supported at r=0 like an umbrella. In the deformed configuration, the sheet is a cone where each cross section looks like a q-lobed flower (q=4 is shown in the figure). Such conical deformation profiles are described using and out-of-plane displacement $w=rg(\theta)$. The paper is divided into two parts: *small deflections*, when $\alpha \ll 1$ leading to linear governing equations, and *finite deflections*, when $\alpha \sim O(1)$, resulting in nonlinear governing equations.

The energy functional to be minimized is,

$$F[g] = E_b - W_{ext} - \lambda I,\tag{7}$$

where λ is the Lagrange multiplier. Next, we compute the variation of the functional δF and set it to zero.

$$\delta E_{b} = B \log \frac{R}{\epsilon} \left[(g'' + g)\delta g'|_{0}^{2\pi} - (g''' + g')\delta g|_{0}^{2\pi} + \int_{0}^{2\pi} d\theta (g^{IV} + g'')\delta g + \int_{0}^{2\pi} d\theta (g + g'')\delta g \right].$$
(8)

g and its derivatives are continuous at $\theta = 0, 2\pi$, which obliterates the boundary terms. Hence,

$$\delta E_b = B \log \frac{R}{\epsilon} \int_0^{2\pi} d\theta \, (g^{IV} + 2g'' + g) \delta g. \tag{9}$$

Similarly,

$$\delta I = -\int_0^{2\pi} d\theta \ (g + g'') \delta g, \qquad \delta W_{ext} = P \int_0^{2\pi} d\theta \ \delta g. \tag{10}$$

Plugging Eqs. (9) and (10) into Eq. (7) gives,

$$0 = \delta F = \int_0^{2\pi} d\theta \left[B \log \frac{R}{\varepsilon} (g^{IV} + 2g'' + g) + \lambda (g'' + g) - P \right] \delta g. \tag{11}$$

This gives us our governing equation for the conical plate.

$$g^{IV} + (2 + \beta)g'' + (1 + \beta)g - P/a = 0, (12)$$

where $a = B \log \frac{R}{\epsilon}$, $\beta = \lambda/a$. The solution to the above equation is,

$$g(\theta) = A\cos q\theta + B\sin q\theta + C\sin\theta + D\cos\theta + \frac{P}{a^2a}.$$
 (13)

where $q=\sqrt{1+\frac{\lambda}{a}}$, and A,B,C,D are constants. Note that the above solution is valid only for small displacements. Our next task to find A,B,C,D,k and λ , which is accomplished by using: (i) periodicity of g, (ii) fixing the origin such that $d\kappa_{\theta}/d\theta=0$, and (iii) inextensibility of the sheet (Eq. (6)). Since the solution is continuous at $\theta=0,2\pi$ and periodic with a period of 2π , $\cos q\theta=\cos q(\theta+2\pi)$ which implies $q\in Z$ must be an integer. We substitute Eq. (13) in Eq. (2) to calculate the curvature.

$$\kappa_{\theta} = -\frac{g'' + g}{r} = \frac{1}{r} (A(q^2 - 1)\cos q\theta + B(q^2 - 1)\sin q\theta - \frac{P}{\sigma^2 q}). \tag{14}$$

Without loss of generality assume $\kappa' = 0$ at $\theta = 0$. This gives B = 0. Next, substitute the expression for $g(\theta)$ in the inextensibility constraint (Eq. (6)), which gives,

$$A = \frac{P}{q^2 a} \sqrt{\frac{2}{q^2 - 1}}. (15)$$

Table 1
Some symbols used in Section 3 for ready reference.

Symbol	Description
В	$\frac{Eh^3}{12(1-v^2)}$
λ	Lagrange multiplier corresponding to the inextensibility constraint
R	Outer radius of the sheet
ε	Size of the boundary layer around the singularity
a	$B \log \frac{R}{\epsilon}$
q	$q = \sqrt{1 + \lambda/a}$, number of folds
β	λ/a
P	$\int_{\varepsilon}^{R} p(r)r^{2}dr$
0'	$\partial/\partial\theta$

This expression gives the amplitude of the folds in terms of the number of folds q. Notice that this form precludes the values q=0,1 since the amplitude blows up. We now calculate the potential energy (PE) to determine the number of folds [3]:

$$PE = U_b - W_{ext} = -\frac{\pi P^2}{a^2 a}.$$
 (16)

Now q is an integer, but $q \neq 0,1$ because the amplitude in Eq. (15) blows up, hence the global minimum of the potential energy occurs at q=2. Thus, q=2 is energetically favorable. However, if we somehow force the sheet to be in a configuration described by q>2 the amplitude is given by Eq. (15).

4. Part 2: Finite deflections

In this section, we solve the problem posed in Section 3 for finite displacements *i.e.* $\alpha \sim O(1)$ (see Fig. 1). We assume that our inextensible sheet is planar in the reference configuration. Here too, we focus on conical configurations isometric to a planar sheet. The sheet is parametrized by a set of two convected coordinates r and θ , as shown in Fig. 2.

We aim to investigate isometric conical solutions of the form $w(r,\theta)=rg(\theta)$ in case of finite displacements. We substitute $w=rg(\theta)$ in the nonlinear von-Kármán plate equations [1] and determine the nature of the external force $p(r,\theta)$ that would admit a conical solution.

We follow the development in Cerda and Mahadevan [4]. The first von Karman equation is:

$$B\Delta^{2}w - \sigma_{rr}\frac{\partial^{2}w}{\partial r^{2}} - \frac{2}{r}\sigma_{r\theta}(\frac{\partial}{\partial r} - \frac{1}{r})\frac{\partial w}{\partial \theta} - \frac{1}{r^{2}}\sigma_{\theta\theta}(\frac{\partial^{2}w}{\partial \theta^{2}} + r\frac{\partial w}{\partial r}) = F_{N}, \quad (17)$$

where $\sigma_{\theta\theta}, \sigma_{r\theta}$ and σ_{rr} are the indeterminate in-plane stresses, $\Delta = \frac{\partial^2}{\partial r^2} + \frac{1}{r} \frac{\partial}{\partial r} + \frac{1}{r^2} \frac{\partial^2}{\partial \theta^2}$, $B = \frac{E t^3}{12(1-v^2)}$ and F_N is the normal force per unit

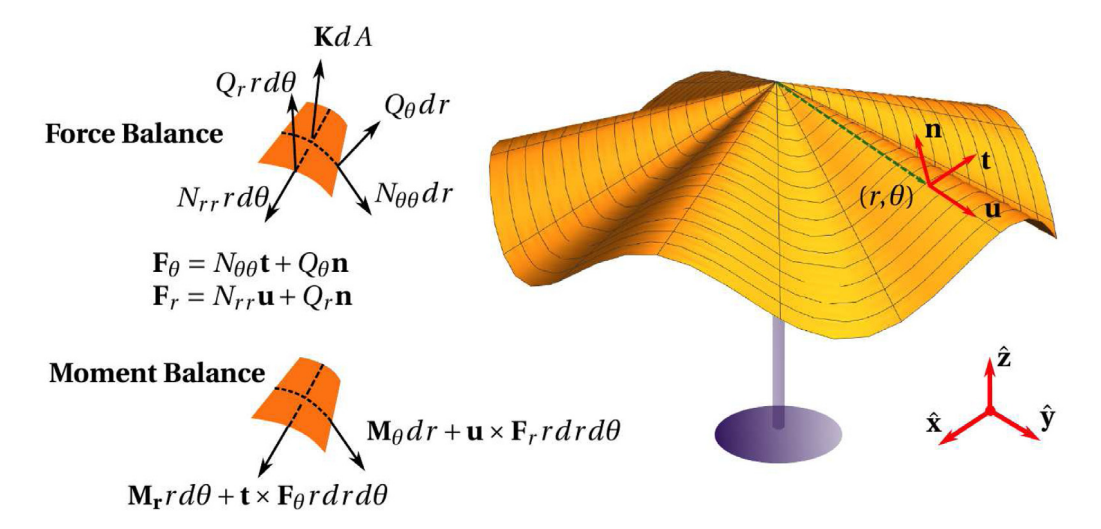


Fig. 2. The sheet is parametrized by convected coordinates r and θ as shown in Fig. 1. At every point (r, θ) , we define a right-handed orthonormal frame [**u**, **t**, **n**]. Here, **u** is the unit vector pointing from tip to the point (r, θ) , **t** is another unit vector tangent to the deformed surface perpendicular to **r**, and **n** is normal to the deformed surface. The external loading of the form $b_n = -\frac{P}{r^2}$ **n**. The position vector of the point (r, θ) in the deformed surface is $\mathbf{r}(r, \theta) = r\mathbf{u}(\theta)$. We show the forces and moments on the two faces defined by **u** and **t**, for an infinitesimal area $dA = rdrd\theta$, which after some algebraic manipulation leads to our governing equations (Eq. (25)). A complete derivation is available in Cerda and Mahadevan [3].

area. Substituting $w = rg(\theta)$ in Eq. (17) we get,

$$g^{IV} + (2 - \frac{\sigma_{\theta\theta}r^2}{B})g'' + (1 - \frac{\sigma_{\theta\theta}r^2}{B})g = \frac{F_N r^3}{B}.$$
 (18)

The governing equation for small displacement is $g^{IV} + (2 + \beta)g'' + (1 + \beta)g = P/a$ (Eq. (12)). Comparing both the equations gives

$$\beta = -\frac{\sigma_{\theta\theta}r^2}{B}, \qquad F_N = \frac{P}{r^3}.$$
 (19)

We show in the following that we can indeed find analytical solutions for the shape of the sheet if the external force decays as $1/r^3$. We give an energy argument to justify the $1/r^3$ assumption in the Appendix.

4.1. Analysis

Let $\mathbf{r}(r,\theta)$ denote the position vector of the point (r,θ) on the sheet in the deformed configuration. We give the symbols used in this section in Table 2. For a conical profile,

$$\mathbf{r}(r,\theta) = r\mathbf{u}(\theta),\tag{20}$$

where $\mathbf{u}(\theta)$ is the unit vector pointing from the tip (or the apex of the cone) to (r,θ) . Next, we compute the gradient vectors $\mathbf{g}_r = \frac{\partial \mathbf{r}}{\partial r} = \mathbf{u}$ and $\mathbf{g}_\theta = \frac{\partial \mathbf{r}}{\partial \theta} = r\mathbf{u}' = r\mathbf{t}$ in the deformed configuration [3], where ()' denotes $\frac{\partial \mathbb{O}}{\partial \theta}$. The normal to the sheet in the deformed configuration is defined as $\mathbf{n} = \mathbf{u} \times \mathbf{u}'$ (see Fig. 2 for the geometry). This set up is used to calculate the components of the first fundamental form $g_{rr}, g_{r\theta}$ and $g_{\theta\theta}$, and the second fundamental form $b_{rr}, b_{r\theta}$ and $b_{\theta\theta}$ [25],

$$g_{rr} = \mathbf{g}_r \cdot \mathbf{g}_r = 1, \quad g_{r\theta} = \mathbf{g}_r \cdot \mathbf{g}_\theta = 0, \quad g_{\theta\theta} = \mathbf{g}_\theta \cdot \mathbf{g}_\theta = r^2,$$
 (21)

and.

$$b_{rr} = -\mathbf{n} \cdot \frac{\partial^{2} \mathbf{r}}{\partial r^{2}} = 0, \quad b_{r\theta} = -\mathbf{n} \cdot \frac{\partial^{2} \mathbf{r}}{\partial r \partial \theta} = -\mathbf{n} \cdot \mathbf{u}' = 0,$$

$$b_{\theta\theta} = -\mathbf{n} \cdot \frac{\partial \mathbf{r}}{\partial \theta^{2}} = -r\mathbf{u} \cdot \mathbf{u}'' = r\kappa.$$
(22)

In the above, $\kappa = -\mathbf{u}.\mathbf{u}''$. The normal curvatures for the sheet $\kappa_{rr}, \kappa_{r\theta}$, and $\kappa_{\theta\theta}$ comprising the second fundamental form (see Ref. [3]) are computed as follows [25]:

$$\kappa_r = \frac{b_{rr}}{g_{rr}} = 0, \quad \kappa_\theta = \frac{b_{\theta\theta}}{g_{\theta\theta}} = \frac{\kappa}{r}, \quad \kappa_{r\theta} = \frac{b_{r\theta}}{g_{r\theta}} = 0.$$
(23)

Table 2
Some symbols used in Section 4 for ready reference.

Symbol	Description
0'	$\partial/\partial\theta$
g_r, g_θ	Gradient vectors for the surface in the deformed state.
В	$\frac{Eh^3}{12(1-v^2)}$
$g_{rr}, g_{\theta\theta}, g_{r\theta}$	Components of metric tensor
$\kappa_r, \kappa_\theta, \kappa_{r\theta}$	Curvatures for the sheet
κ	$r\kappa_{ heta}$
$b_n = P/r^3$	External force acting normal to the elastic sheet
p	P/B
$W, Q, m, y_1, y_3, \kappa_0$	Parameters in the solution to κ Eq. (32)
K(k)	Denotes the complete elliptic function
[u, t, n]	Orthonormal frame at the point r, θ .
$N_{rr}, N_{\theta\theta}, Q_r, Q_{\theta}$	Contact forces
$\mathbf{M}_{\theta}, \mathbf{M}_{r}$	Contact moments

 $\kappa_\theta,\,\kappa_r$ and $\kappa_{r\theta}$ are related linearly to the moments in the sheet m_r,m_θ and $m_{r\theta}$ [3]:

$$m_r = B(\kappa_r + \nu \kappa_\theta) = B\nu \frac{\kappa}{r}, \quad m_\theta = B(\kappa_\theta + \nu \kappa_r) = B\frac{\kappa}{r},$$

$$m_{r\theta} = B(1 - \nu)\kappa_{r\theta} = 0,$$
(24)

where v is the Poisson ratio, E is the Young's modulus, and $B = \frac{Eh^3}{12(1-v^2)}$.

We use the force balance and moment balance equations for the sheet derived by Cerda and Mahadevan [3]:

$$\frac{\partial \mathbf{F}_{\theta}}{\partial \theta} + \frac{\partial (r\mathbf{F}_{r})}{\partial r} + r\mathbf{K} = 0,
\frac{\partial \mathbf{M}_{\theta}}{\partial \theta} + \frac{\partial (r\mathbf{M}_{r})}{\partial r} + r(\mathbf{t} \times \mathbf{F}_{\theta} + \mathbf{u} \times \mathbf{F}_{r}) = 0.$$
(25)

Here, \mathbf{F}_{θ} and \mathbf{F}_{r} denote the force per unit length on the cross section defined by θ =constant and r = constant, respectively. \mathbf{M}_{θ} and \mathbf{M}_{r} are defined similarly. \mathbf{K} is the loading per unit reference area. In the $[\mathbf{u}, \mathbf{t}, \mathbf{n}]$ orthonormal frame,

$$\begin{split} \mathbf{M}_{\theta} &= \mathbf{n} \times (m_{\theta\theta}\mathbf{t} + m_{r\theta}\mathbf{u}) = B\frac{\kappa}{r}\mathbf{u}, \quad \mathbf{M}_{r} = \mathbf{n} \times (m_{rr}\mathbf{u} + m_{r\theta}\mathbf{t}) = -\nu B\frac{\kappa}{r}\mathbf{t}, \\ \mathbf{F}_{\theta} &= N_{\theta\theta}(r,\theta)\mathbf{t} + Q_{\theta}(r,\theta)\mathbf{n}, \quad \mathbf{F}_{r} = Q_{r}(r,\theta)\mathbf{n} + N_{rr}(r,\theta)\mathbf{u}, \\ \mathbf{K} &= b_{n}\mathbf{n}. \end{split}$$

Since, [u,t,n] constitutes a right handed coordinate system, it follows that [3].

$$\mathbf{u}' = \mathbf{t}, \quad \mathbf{t}' = -\kappa \mathbf{n} - \mathbf{u}, \quad \mathbf{n}' = \kappa \mathbf{t}.$$
 (27)

We substitute Eqs. (26) and (27) back into the equilibrium equations (Eq. (25)), and get the following equations:

$$\begin{split} \frac{\partial N_{\theta\theta}}{\partial \theta} + \kappa Q_{\theta} &= 0, \quad (a) \quad \frac{\partial (rN_{rr})}{\partial r} - N_{\theta\theta} &= 0, \quad (b) \\ \frac{\partial Q_{\theta}}{\partial \theta} + \frac{\partial (rQ_{r})}{\partial r} - \frac{\partial (rN_{\theta\theta})}{\partial r} + rb_{n} &= 0, \quad (c) \end{split} \tag{28}$$

and

$$Q_{\theta} = \frac{B\kappa'}{r^2}, \qquad Q_r = -\frac{B\kappa}{r^2}. \tag{29}$$

Eliminating Q_{θ} and Q_r using Eq. (29) from Eq. (28)(a) gives $N'_{\theta\theta} + \kappa B\kappa''/r^2 = 0$. Integrating the equation yields $N_{\theta\theta} = -B(\kappa^2/2r^2 + \frac{\partial \psi(r)}{\partial r})$, for some function $\psi(r)$. Substituting this expression for $N_{\theta\theta}$ and Q_{θ} and Q_r from Eq. (29) into Eq. (28)(c), we get $B\left[\kappa'' + \kappa^3/2\right] + B\kappa(1 + r^2\frac{\partial \psi}{\partial r}) + r^3b_n(r) = 0$. From Eq. (19), we know that $b_n = \frac{P}{r^3}$. Hence our governing equation for κ is,

$$B\left[\kappa'' + \kappa^3/2\right] + B\kappa(1 + r^2\frac{\partial\psi}{\partial r}) + P = 0,$$
(30)

which can be rewritten as $\left[\frac{B}{\kappa}(\kappa'' + \kappa^3/2) + \frac{P}{\kappa}\right] = -B(1 + r^2\frac{\partial \psi}{\partial r})$. The RHS is a function of r while the LHS is a function of θ . This enables us to separate variables, wherein both sides are equal to a constant. Let $(1 + r^2\frac{\partial \psi}{\partial r}) = \sigma$, then,

$$\kappa'' + \kappa^3 / 2 - \sigma \kappa + p = 0, \tag{31}$$

where $p = \frac{P}{B}$. This nonlinear differential equation can be solved (eq. 1 in [26]). We begin by integrating the equation to obtain,

$$\frac{\kappa'^2}{2} + \frac{\kappa^4}{8} - \frac{\sigma \kappa^2}{2} + p\kappa = C,\tag{32}$$

where C is the constant of integration. We fix the origin such that $\kappa'=0$ and $\kappa=\kappa_0$ at $\theta=0$. We can then eliminate C and introduce another constant κ_0 which has a physical meaning. To integrate Eq. (32), we change the variable to $y=\frac{1}{\kappa_0-\kappa}$, then,

$$\int_{y}^{\infty} \frac{1}{\sqrt{y^{3} + \frac{Q}{W}y^{2} + \frac{\kappa_{0}}{W}y - \frac{1}{dW}}} = \int_{s}^{0} \sqrt{W} d\theta, \tag{33}$$

where

$$W = \kappa_0^3 - 2\sigma\kappa_0 + 2p, \qquad Q = -3\kappa_0^2/2 + \sigma.$$
 (34)

Hence, $W+2\kappa_0Q+2\kappa_0^3=2p$. At this stage, p is known while W, Q and κ_0 are the unknowns. Let $y^3+\frac{Q}{W}y^2+\frac{\kappa_0}{W}y-\frac{1}{4W}=(y-\alpha)[(y-m)^2+n^2]$

Then, the solution to Eq. (31) can be expressed in the form of Jacobi elliptic functions as follows,

$$\kappa(\theta) = \kappa_0 - \frac{1 - \text{cn}\left(-\frac{\sqrt{W(y_1 - y_3)}}{\sqrt{2}}\theta \middle| \sqrt{\frac{m - y_3}{y_1 - y_3}}\right)}{y_1 - y_3 \text{cn}\left(-\frac{\sqrt{W(y_1 - y_3)}}{\sqrt{2}}\theta \middle| \sqrt{\frac{m - y_3}{y_1 - y_3}}\right)},$$
(35)

where y_1 and y_3 are the roots of $y^2 - 2\alpha y + 2m\alpha - (m^2 + n^2)$, $\operatorname{cn}(x|k)$ is a Jacobi Elliptic function [24]. The constants κ_0 , W and Q can be expressed in terms of m, y_1 and y_3 .

$$\kappa_0 = \frac{2m - \frac{y_1 y_3}{y_1 + y_3}}{2m(y_1 + y_3) - 2y_1 y_3}, \quad W = \frac{(y_1 + y_3)\kappa_0 - 0.5}{m(y_1 + y_3)^2},$$

$$Q = -W\left(2m + \frac{y_1 + y_3}{2}\right).$$
(36)

Now, we have four unknown parameters y_1 , y_3 , κ_0 and m in the solution (Eq. (35)). We need four equations to evaluate them which are as follows:

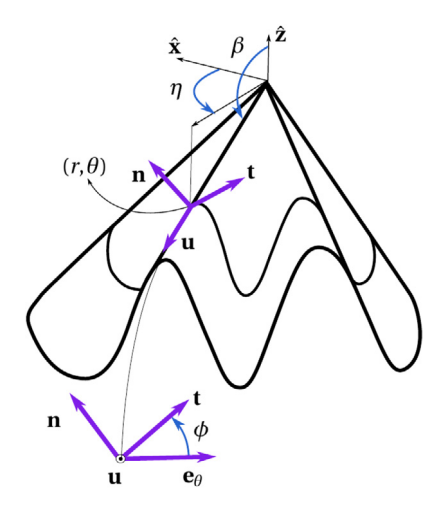


Fig. 3. Conical geometry of the elastic plate in the deformed configuration. Here $\mathbf{u}=\sin\beta\cos\eta~\hat{\mathbf{x}}+\sin\beta\sin\eta~\hat{\mathbf{y}}+\cos\beta~\hat{\mathbf{z}},~\mathbf{e}_{\theta}=\cos\eta~\hat{\mathbf{x}}+\sin\eta~\hat{\mathbf{y}}.$ Now $\mathbf{t}=\mathbf{u}'=\cos\phi\mathbf{e}_{\theta},$ also $\mathbf{n}=\mathbf{u}\times\mathbf{t}=-\sin\phi~\hat{\mathbf{x}}+\cos\phi~\hat{\mathbf{y}}.$ These equalities lead to the geometric relations in Eq. (41).

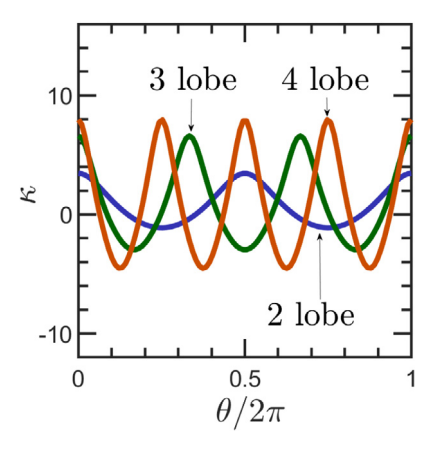


Fig. 4. Plot of curvature κ vs θ for q=2,3, and 4 lobed configurations using Eq. (35). Notice that the solutions are periodic but not sinusoidal as in case of small displacements.

1. Algebraic relation between W, Q and κ_0 : This relation can be got from Eq. (34).

$$W + 2\kappa_0 Q + 2\kappa_0^3 = 2p. (37)$$

p=P/B is the applied loading. Then, we use $W=\frac{(y_1+y_3)\kappa_0-0.5}{m(y_1+y_3)^2}$ and $Q=-W\left(2m+\frac{y_1+y_3}{2}\right)$ from Eq. (36) to eliminate W and Q.

2. Continuity of the curvature κ : The Jacobi elliptic function $\operatorname{cn}(x|k)$ is periodic: $\operatorname{cn}(\theta|k) = \operatorname{cn}(\theta + 4qK(k)|k)$ where K(k) is the complete elliptic integral of first kind and q is an integer. To ensure the continuity of the curvature, we impose $\kappa(2\pi) = \kappa_0 = \kappa(0)$. We will eventually see that q denotes the number of folds in the sheet. Hence,

$$\sqrt{\frac{W(y_1 - y_3)}{2}} 2\pi = 4qK\left(\sqrt{\frac{m - y_3}{y_1 - y_2}}\right). \tag{38}$$

Using $W = \frac{(y_1 + y_3)\kappa_0 - 0.5}{m(y_1 + y_3)^2}$ from Eq. (36) gives

$$\frac{2(4qK)^2}{(y_1 - y_3)(2\pi)^2} - \frac{(y_1 + y_3)\kappa_0 - 0.5}{m(y_1 + y_3)^2} = 0.$$
 (39)

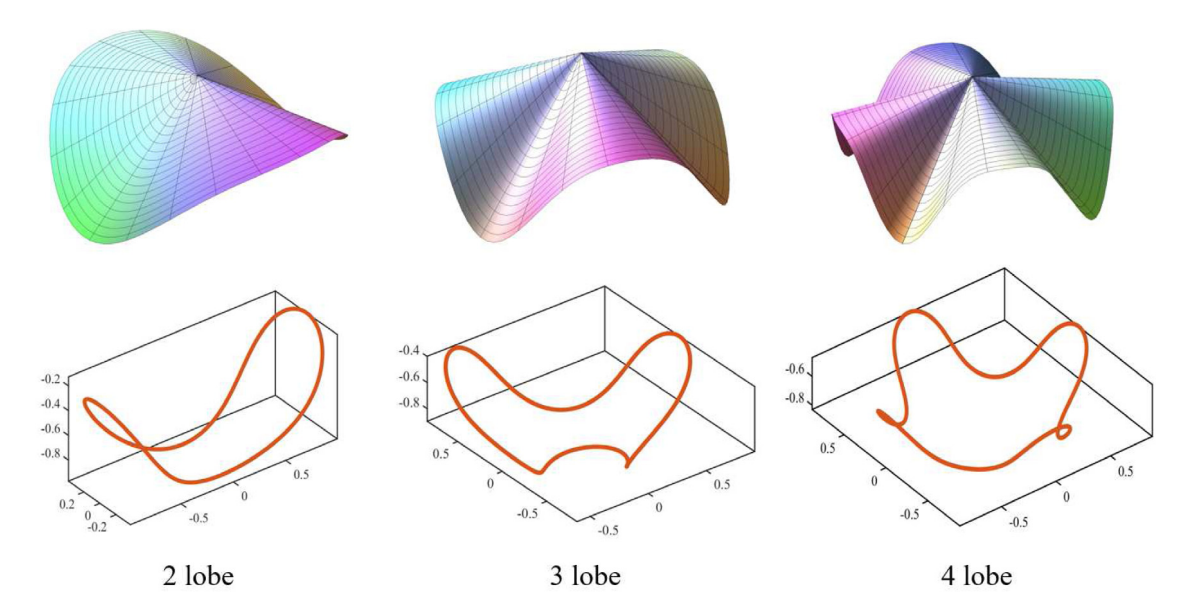


Fig. 5. We integrate Eq. (35) to get the deformed shapes for q = 2,3, and 4 lobed configurations. p = -3.5 for two lobed solution, p = -9.0 for three lobed solution, and p = -16.0 for four lobed solution. The top plots show the shape of the deformed plate. The bottom plots show the deformed shape of the circle r = 1.

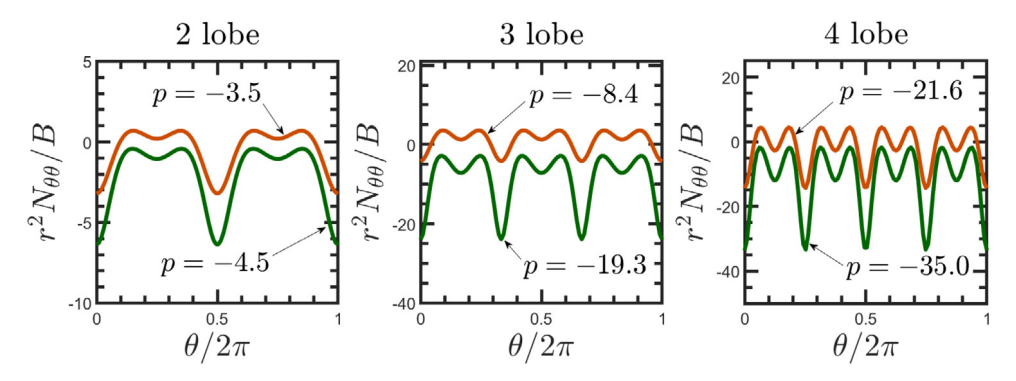


Fig. 6. The plots for $N_{\theta\theta} = -N_{rr} = -\frac{B}{2}(\frac{\kappa^2}{2} + \frac{3\kappa_0^2}{2} + Q - 1)$ for q = 2, 3, and 4 lobed configurations for various values of loading p.

3. Algebraic relation between y_1 , y_3 , m and κ_0 : This relation is obtained from Eq. (36).

$$\kappa_0 = \frac{2m - \frac{y_1 y_3}{y_1 + y_3}}{2m(y_1 + y_3) - 2y_1 y_3}.$$
(40)

4. *Azimuthal symmetry*: This condition relates to the symmetry of the deformed shape of the elastic sheet. Consider the elastic sheet shown in Fig. 3, the angles η , β , and θ describe the conical profile such that $\mathbf{u} = \sin \beta \cos \eta \ \hat{\mathbf{x}} + \sin \beta \sin \eta \ \hat{\mathbf{y}} + \cos \beta \ \hat{\mathbf{z}}$, where $\hat{\mathbf{x}}$, $\hat{\mathbf{y}}$, $\hat{\mathbf{z}}$ are unit vectors in a lab frame (see Fig. 2). The following relations can be computed by using the conical geometry [3], as shown in Fig. 3,

$$\beta' = -\sin\phi,$$

$$\eta' = \frac{\cos\phi}{\sin\beta},$$
(41)

 $\phi' = \kappa - \cot \beta \cos \phi.$

For a q-lobed solution, the three boundary conditions necessary to solve the above system are $\beta(0) = \beta(2\pi/q)$, $\phi(0) = \phi(2\pi/q)$, and $\eta(0) = 0$. The fourth condition required to evaluate the four constants y_1, y_3, m and κ_0 is,

$$\eta(2\pi/q) = 2\pi/q. \tag{42}$$

We need to solve the four equations (37), (39), (40), and (42) to evaluate our four unknown constants y_1, y_3, m and κ_0 . We solve them numerically in MATLAB using Newton's method.

4.2. Results

In this section, we present the results for the geometry, stresses, and elastic energy for q=2,3, and 4 lobed configurations, and comment briefly on their relative stability.

We plot the curvature $\kappa(\theta)$ vs θ for q=2,3, and 4 lobed configurations in Fig. 4. We integrate the curvature κ to compute the actual shapes of the deformed sheets for various lobes, shown in Fig. 5. We would like to understand these different shapes from the perspective of elastic energy and stresses.

Let us compute the stresses $N_{\theta\theta}$ and N_{rr} in the sheets. From Eq. (28), we get $N_{\theta\theta} = -B(\kappa^2/2r^2 + \frac{\partial \psi(r)}{\partial r})$, which in terms of W,Q and κ_0 is,

$$N_{\theta\theta} = -\frac{B}{r^2} \left(\frac{\kappa^2}{2} + \frac{3\kappa_0^2}{2} + Q - 1 \right). \tag{43}$$

We plot $r^2N_{\theta\theta}/B$ in Fig. 6 for q=2,3, and 4 lobed solutions, and find that it is periodic in θ . The amplitude of the oscillation increases as the magnitude of the external force p increases. Furthermore, we can compute N_{rr} from Eq. (28), $N_{rr}=\frac{B}{r^2}\Big(\frac{\kappa^2}{2}+\frac{3\kappa_0^2}{2}+Q-1\Big)=-N_{\theta\theta}$. Hence, the behavior of N_{rr} is similar to $N_{\theta\theta}$.

Next we compute the potential energy PE of for q=2,3 and 4 lobed shapes, which consists of the elastic energy E_b , and the work done by the external loading W_e .

$$PE = E_b - W_o. (44)$$

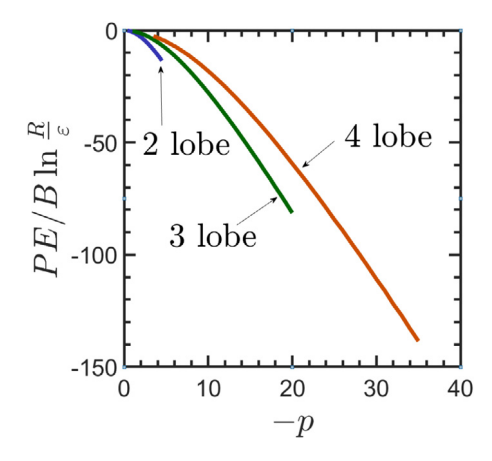


Fig. 7. Potential energy (PE) of the elastic sheet versus the loading. The two lobed solution has lowest potential energy. A similar trend was observed in case of small displacements (Section 3). Self contact occurs for a two lobed solution at p = -4.7, for a three lobed solution at p = -21.3, and for a four lobed solution at p = -60.05.

Using Eqs. (3) and (4) we get,

$$E_b = \frac{B}{2} \ln \frac{R}{\epsilon} \int_0^{2\pi} \kappa^2 d\theta \tag{45}$$

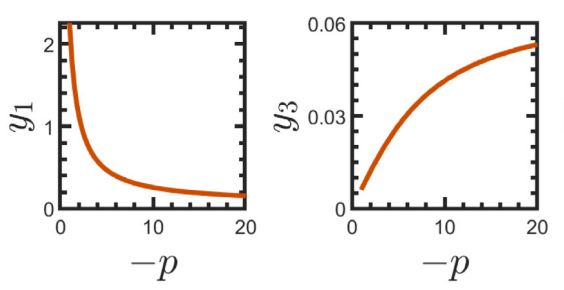
The work done by external loading W_e is,

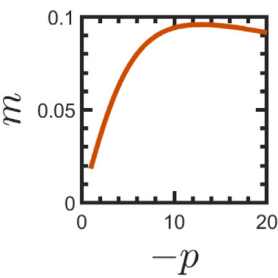
$$W_e = P \ln \frac{R}{\epsilon} \int_0^t dt \int_0^{2\pi} d\theta \, (\dot{\eta} \beta' - \eta' \dot{\beta}) \sin \beta, \tag{46}$$

where $\dot{\eta} = \frac{d\eta}{dt}$. A derivation for the above result is given in the Appendix. We plot the *PE* versus p = P/B in Fig. 7 for q = 2,3 and 4 lobed configurations. In Section 3, where we assumed small displacements, we concluded that as the number of lobes increases the potential energy of the elastic sheet increases (Eq. (16)), which, as Fig. 7 demonstrates, holds true for large displacements as well. The self contact for 2, 3 and 4 lobed configurations occurs at p = -4.7, -21.3 and -60.0, respectively.

Finally, we show that, as the external force $p \to 0$, the solution to the curvature for large displacements in the form of elliptic functions (Eq. (35)) is equivalent to the sinusoidal solution obtained by assuming small displacements (Eq. (14)). We plot the variation of the parameters y_1, y_3, m and κ_0 in Eq. (35) with the external load p in Fig. 8. We observe that as, $p \to 0$, $y_3, m, \kappa_0 \to 0$, $m - y_3 > 0$, and $y_1 \to \infty$. Using these trends, we conclude that $\sqrt{\frac{m-y_3}{y_1-y_3}} \to 0$. Hence from Eq. (38) and

$$\begin{split} K\left(\sqrt{\frac{m-y_3}{y_1-y_3}}\right) &\to \frac{\pi}{2}, \quad \sqrt{\frac{W(y_1-y_3)}{2}} = \frac{4qK}{2\pi} \to q, \\ &\operatorname{cn}\left(\sqrt{\frac{W(y_1-y_3)}{2}}\theta | \sqrt{\frac{m-y_3}{y_1-y_3}}\right) \to \cos q\theta. \end{split}$$





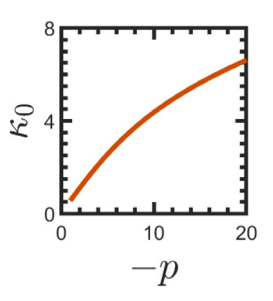


Fig. 8. Trends in the parameters in the curvature $\kappa(\theta) = \kappa_0 - \frac{1-\mathrm{cn}\left(-\frac{\sqrt{W(t_1-y_1)}}{\sqrt{2}}\theta\left|\sqrt{\frac{m-y_1}{y_1-y_2}}\right|\right)}{y_1-y_3\mathrm{cn}\left(-\frac{\sqrt{W(t_1-y_1)}}{\sqrt{y_1-y_2}}\theta\left|\sqrt{\frac{m-y_1}{y_1-y_2}}\right|\right)}$ (Eq. (35)) for q=3. Using these trends we show that as $p\to 0$, the above expression for $\kappa(\theta)$ in the form of Jacobi elliptic functions is equivalent to the sinusoidal solution $\kappa(\theta) = \frac{p}{k^2}(\sqrt{2(k^2-1)}\cos q\theta-1)$ obtained by assuming small displacement (Eq. (14))

Hence.

$$\kappa(\theta) = \kappa_0 - \frac{1 - \text{cn}\left(-\frac{\sqrt{W(y_1 - y_3)}}{\sqrt{2}}\theta \middle| \sqrt{\frac{m - y_3}{y_1 - y_3}}\right)}{y_1 - y_3 \text{cn}\left(-\frac{\sqrt{W(y_1 - y_3)}}{\sqrt{2}}\theta \middle| \sqrt{\frac{m - y_3}{y_1 - y_3}}\right)} \to \alpha_1 + \alpha_2 \cos q\theta. \tag{47}$$

where, $\alpha_1 \approx \kappa_0 - \frac{1}{y_1}$ and $\alpha_2 \approx \frac{1}{y_1}$. Furthermore, $\alpha_1, \alpha_2 \to 0$ as $p \to 0$, which matches with Eq. (14).

5. Conclusion

We investigated the deformations of a flat inextensible elastic sheet subjected to an external distributed load which acts in the direction normal to the sheet in the deformed configuration. The deformed shape of the sheet is a characteristic q- lobed conical shape with zero Gauss curvature everywhere except at the apex, which is a singularity. In Section 3, we assumed that the displacements are small. Consequently, the curvature of the sheet is sinusoidal in the angular convected coordinate θ . We found that for a given load, q=2 lobed configuration has the lowest potential energy, and as the number of lobes increases, the potential energy also increases. In Section 4, we allow for arbitrarily large displacements, thus the governing equations for the curvature are nonlinear. Nevertheless, we found an analytical solution in the form of Jacobi elliptic functions. We observe that in this case, the curvature and stresses are periodic but not sinusoidal. In this case too, the 2-lobed solution has the lowest potential energy, but it reaches self-contact at a small load. Finally, we showed that in the limit of small loads our solution for the curvature in the form of Jacobi elliptic function for large displacements (Eq. (35)) is equivalent to the sinusoidal solution obtained for the small displacements (Eq. (14)). Although, our analysis is valid only if the external load decays as $1/r^3$, the analytical solutions can be useful benchmarks for computational methods aimed at calculating shapes of highly deformed elastic sheets. Some ideas in our solutions may also be utilized to compute shapes of sheets under periodic (in θ) external loading.

Acknowledgments

We acknowledge support from NSF grant NSF CMMI 1662101. This problem was conceived in a course on rods and shells taught by John L. Bassani at the University of Pennsylvania.

Appendix A. Computation of work done by external loading

We compute the work done by external loading $\frac{P}{r^3}$ **n** required in Eq. (44). Let us introduce a time variable t, such that the elastic sheet is in the reference configuration at t=0 and deforms as t increases. The position vector of the point (r,θ) in the deformed configuration is $\mathbf{r} = r\mathbf{u}(\theta,t)$, where

$$\mathbf{u} = \sin \beta \cos \eta \ \hat{\mathbf{x}} + \sin \beta \sin \eta \ \hat{\mathbf{y}} + \cos \beta \ \hat{\mathbf{z}}, \tag{A.1}$$

as shown in Fig. 3. Now $\beta = \beta(\theta, t)$ and $\eta = \eta(\theta, t)$. The work done by the external force $p(r, \theta) = \frac{P}{3}$ n is computed as follows,

$$W_e = \int_0^t dt \left(\int_{\varepsilon}^R dr \int_0^{2\pi} r d\theta \, \frac{d(r\mathbf{u})}{dt} \cdot \frac{P}{r^3} \mathbf{n} \right) = P \ln \frac{R}{\varepsilon} \int_0^t dt \int_0^{2\pi} d\theta \, \frac{d\mathbf{u}}{dt} \cdot \mathbf{n},$$
(A.2)

We use Eq. (A.1) to compute $\frac{d\mathbf{u}}{dt}$. Now $\mathbf{t} = \frac{d\mathbf{u}}{d\theta}$ and $\mathbf{n} = \mathbf{u} \times \mathbf{t}$. Performing these computations gives,

$$\frac{d\mathbf{u}}{dt}.\mathbf{n} = \sin\beta \ (\dot{\eta}\beta' - \eta'\dot{\beta}),\tag{A.3}$$

where $\dot{(}) = \frac{d}{dt}$ and $()' = \frac{d}{d\theta}$.

Appendix B. Boundedness of the potential energy

In this paper we assumed that the external load $p(r,\theta)$ is independent of θ , and furthermore $p(r) \propto \frac{1}{r^3}$, which results in a convenient variable separation allowing us to solve the problem analytically. While a facile reason for choosing $p(r) \propto \frac{1}{r^3}$ is to simplify the problem, there is a deeper insight involving the singularity at the apex of the d- cone. Let $0 < r < \varepsilon$ be the region around the apex where our assumption that the sheet is inextensible is not valid. A cavalier approach to avoid the singularity (as we have done in this paper) is to discard the isometric solution when $0 < r < \varepsilon$ as it leads to a logarithmic divergence of the total elastic energy of the plate. To prevent this, the sheet stretches near the apex when $0 < r < \varepsilon$, violating the isometry. Under these considerations, the total energy of the sheet E_n is,

$$E_p = E_{\varepsilon < r < R} + E_{0 < r < \varepsilon},$$

where $E_{\varepsilon < r < R}$ consists of only bending elastic energy in the region $\varepsilon < r < R$, and $E_{0 < r < \varepsilon}$ consists of both bending and stretching elastic energy in the region $0 < r < \varepsilon$. Minimizing E_p leads to a scaling law for ε that depends on the thickness of the sheet h and outer radius of the sheet R: $\varepsilon \sim h^{1/3} R^{2/3}$ [27,28]. While this scaling law assures that for a thin sheet $(h \rightarrow 0)$, the size of the singularity $\varepsilon \rightarrow 0$, it leads to another conundrum — the elastic energy $E_b = B \ln \frac{R}{\rho} \int_0^{2\pi} \kappa^2 d\theta$ diverges (Eq. (44) of the main text). To resolve this, we use Theorem 1 in Müller and Olbermann [22] which proves that the total energy (bending + stretching) is bounded for deformations of the conical plate that are determined entirely by those on the one-dimensional boundary (as in our case and that in Cerda and Mahadevan [3]). However, Müller and Olbermann [22] did not consider the potential energy from the work done by external load. This is where our hypothesis that the external load decays as $1/r^3$ is essential. Under this assumption the contribution arising out of integration along the radial coordinate racts as multiplicative constant for the entire potential energy PE (see below).

$$\begin{split} PE &= E_b - W_e \\ &= B \int_{\varepsilon}^R dr \int_0^{2\pi} r d\theta \ \kappa_\theta^2 - \int_0^t dt \Big(\int_{\varepsilon}^R dr \int_0^{2\pi} r d\theta \ \frac{d(r\mathbf{u})}{dt} \cdot \frac{P}{r^3} \mathbf{n} \Big) \\ &= B \int_{\varepsilon}^R dr \int_0^{2\pi} r d\theta \ \frac{\kappa^2}{r^2} - \int_0^t dt \Big(\int_{\varepsilon}^R dr \int_0^{2\pi} r d\theta \ \frac{d(r\mathbf{u})}{dt} \cdot \frac{P}{r^3} \mathbf{n} \Big) \\ &= \int_{\varepsilon}^R dr \frac{1}{r} \Big(B \int_0^{2\pi} d\theta \ \kappa^2 - P \int_0^t dt \int_0^{2\pi} d\theta \ \frac{d\mathbf{u}}{dt} \cdot \mathbf{n} \Big) \\ &= C \int_{\varepsilon}^R dr \frac{1}{r} \end{split}$$

where $C = \left(B \int_0^{2\pi} d\theta \quad \kappa^2 - P \int_0^{2\pi} d\theta \quad \int_0^t dt \, \frac{d\mathbf{u}}{dt} \cdot \mathbf{n}\right)$ is constant, just as in Cerda and Mahadevan [3] in which there is no external load. Note that this multiplicative decomposition happens only if the external force $p(r) \propto \frac{1}{r^3}$. With a potential energy of this form Theorem 1 of Müller and Olbermann [22] guarantees the existence of a minimizer of the energy.

References

- S.P. Timoshenko, S. Woinowsky-Krieger, Theory of Plates and Shells, McGraw-hill, 1959.
- [2] Y.C. Fung, Foundations of Solid Mechanics, Prentice Hall, 2017.
- [3] E. Cerda, L. Mahadevan, Confined developable elastic surfaces: cylinders, cones and the elastica, in: Proceedings: Mathematics, Physical and Engineering, 2005, pp. 671–700.
- [4] E. Cerda, L. Mahadevan, Conical surfaces and crescent singularities in crumpled sheets, Phys. Rev. Lett. 80 (11) (1998) 2358.
- [5] B. Audoley, Y. Pomeau, Elasticity and Geometry, Oxford University Press, 2010.
- [6] M.B. Amar, Y. Pomeau, Crumpled paper, in: Proceedings of the Royal Society of London A: Mathematical, Physical and Engineering Sciences, Vol. 453, No. 1959, The Royal Society, 1997, pp. 729–755.
- [7] E. Cerda, L. Mahadevan, J.M. Pasini, The elements of draping, Proc. Natl. Acad. Sci. 101 (7) (2004) 1806–1810.
- [8] J. Altenbach, H. Altenbach, V.A. Eremeyev, On generalized Cosserat-type theories of plates and shells: a short review and bibliography, Arch. Appl. Mech. 80 (1) (2010) 73–92.
- [9] E. Cerda, L. Mahadevan, Geometry and physics of wrinkling, Phys. Rev. Lett. 90 (7) (2003) 074302.
- [10] H. King, R.D. Schroll, B. Davidovitch, N. Menon, Elastic sheet on a liquid drop reveals wrinkling and crumpling as distinct symmetry-breaking instabilities, Proc. Natl. Acad. Sci. 109 (25) (2012) 9716–9720.
- [11] W. Helfrich, Elastic properties of lipid bilayers: theory and possible experiments, Z. Naturforsch. C 28 (11–12) (1973) 693–703.
- [12] N. Mohandas, E. Evans, Mechanical properties of the red cell membrane in relation to molecular structure and genetic defects, Annu. Rev. Biophys. Biomol. Struct. 23 (1) (1994) 787–818.
- [13] P.B. Canham, The minimum energy of bending as a possible explanation of the biconcave shape of the human red blood cell, J. Theoret. Biol. 26 (1) (1970) 61-81
- [14] J.E. Rim, P.K. Purohit, W.S. Klug, Mechanical collapse of confined fluid membrane vesicles, Biomech. Model. Mechanobiol. 13 (6) (2014) 1277–1288.
- [15] W.M. van Rees, E. Vouga, L. Mahadevan, Growth patterns for shape-shifting elastic bilayers, Proc. Natl. Acad. Sci. (2017) 201709025.
- [16] M.M. Mller, M.B. Amar, J. Guven, Conical defects in growing sheets, Phys. Rev. Lett. 101 (15) (2008) 156104.
- [17] S. Sadik, A. Angoshtari, A. Goriely, A. Yavari, A geometric theory of nonlinear morphoelastic shells, J. Nonlinear Sci. 26 (4) (2016) 929–978.
- [18] S. Miyashita, I. DiDio, I. Ananthabhotla, B. An, C. Sung, S. Arabagi, D. Rus, Folding angle regulation by curved crease design for self-assembling origami propellers, J. Mech. Robot. 7 (2) (2015) 021013.
- [19] J.P. Duncan, J.L. Duncan, Folded developables, Proc. R. Soc. Lond. Ser. A Math. Phys. Eng. Sci. 383 (1784) (1982) 191–205.
- [20] D. Dureisseix, An overview of mechanisms and patterns with origami, Int. J. Space Struct. 27 (1) (2012) 1–14.
- [21] E. Cerda, S. Chaieb, F. Melo, L. Mahadevan, Conical dislocations in crumpling, Nature 401 (6748) (1999) 46.
- [22] S. Müller, H. Olbermann, Conical singularities in thin elastic sheets, Calc. Var. Partial Differential Equations 49 (3–4) (2014) 1177–1186.
- [23] D.L. Blair, A. Kudrolli, Geometry of crumpled paper, Phys. Rev. Lett. 94 (16) (2005) 166107.
- [24] M. Abramowitz, I.A. Stegun, Handbook of Mathematical Functions with Formulas, Graphs, and Mathematical Tables, in: Applied Mathematics Series, vol. 55, National Bureau of Standards, Washington, DC, 1964.
- [25] D.J. Struik, Lectures on Classical Differential Geometry, Dover, New York, 1988.
- [26] S.K. Veerapaneni, R. Raj, G. Biros, P.K. Purohit, Analytical and numerical solutions for shapes of quiescent two-dimensional vesicles, Int. J. Non-Linear Mech. 44 (3) (2009) 257–262.
- [27] E. Cerda, S. Chaieb, F. Melo, L. Mahadevan, Conical dislocations in crumpling, Nature 401 (6748) (1999) 46.
- [28] T.A. Witten, Stress focusing in elastic sheets, Rev. Modern Phys. 79 (2) (2007) 643.